Caenorhabditis elegans **Uses Canonical and Non-canonical Hippo signaling**

Linh Huynh[1], Razan A. Fakieh[1,2], C'Brionne Hendrix[1], Reid Powell[1], David J. Reiner[1,3,§]

[1] College of Medicine, Texas A&M University, Houston TX, 77030, USA

[2] Clinical Laboratory Sciences Department, College of Applied Medical Sciences, Imam Abdulrahman bin Faisal University, Dammam 34212, Kingdom of Saudi Arabia.

[3] Institute of Biosciences and Technology, Texas A&M Health Science Center, Houston TX, 77030, USA

[§] To whom correspondence should be addressed: dreiner@tamu.edu

Key words: Wts, Yki, Hpo, Sterile 20, MST1, MST2, Hippo, Warts, Yap, TEAD, MIG-15, GCK-2

ABSTRACT

Hippo signaling is a conserved regulator of tissue homeostasis across metazoans. The Ste20 family kinase Hippo/MST activates the NDR family kinase Warts/LATS to inhibit the transcriptional coactivator Yorkie/YAP/TAZ and its transcription factor partner Scalloped/TEAD. In *Caenorhabditis elegans*, cell lineages and organ sizes are largely invariant, and classical Hippo phenotypes such as tissue overgrowth are absent. Nevertheless, WTS-1, YAP-1, and the TEAD-like transcription factor EGL-44 form a conserved core module required for larval development past the L2 stage. Crucially, a direct role for Hippo signaling remains unestablished. To address this question, we generated a fluorescently tagged endogenous YAP-1 as a live biomarker of pathway activity. Upon WTS-1 loss, endogenous YAP-1 translocated from cytosol to nucleus in epithelium and intestine. Tissue-specific depletion revealed that intestinal, but not epithelial, WTS-1 is essential for progression past L2. The duplicated Hippo-related kinases CST-1 and CST-2 repressed YAP-1 nuclear localization in the epithelium but not intestine, indicating that intestinal WTS-1 functions without CST-1/2. The Ste20 kinase MIG-15, orthologous to *Drosophila* Misshapen and mammalian MAP4K4/6/7/8, was redundant with CST-1/2 for larval progression. Yet deficient MIG-15 uniquely increased YAP-1 abundance without driving nuclear localization. By contrast, the Ste20 kinase GCK-2, orthologous to *Drosophila* Happyhour and mammalian MAP4K1/2/3/5, had no detectable role. Our findings establish *C. elegans* as a model for Hippo signaling, with a canonical cascade active in the epithelium and noncanonical inputs controlling WTS-1 in the intestine. In this context, YAP-1/EGL-44 outputs are repurposed from growth control to non-proliferative developmental functions.

INTRODUCTION

The Hippo signaling pathway was first discovered in *Drosophila* loss-of-function screens that identified tumor suppressor genes required to prevent tissue overgrowth (JUSTICE *et al.* 1995; TAPON *et al.* 2002; HARVEY *et al.* 2003; WU *et al.* 2003). Subsequent studies revealed that the downstream transcriptional coactivator Yorkie (Yki) is essential to avoid the converse phenotype of tissue undergrowth (HUANG *et al.* 2005). The canonical pathway consists of the Ste20-family (from yeast Sterile 20) kinase Hippo (Hpo; mammalian Mst1/2) phosphorylating and activating the NDR-family kinase Warts (Wts; mammalian LATS1/2), which in turn phosphorylates and represses Yki/YAP/TAZ (HUANG *et al.* 2005; OH AND IRVINE 2010). Phosphorylated Yki/YAP/TAZ is excluded from the nucleus, preventing it from associating with the transcription factor Scalloped (Sd; mammalian TEAD1-4) to drive expression of growth-promoting transcriptional client genes (VASSILEV *et al.* 2001; WU *et al.* 2008; ZHANG *et al.* 2008), reviewed in (HALDER AND JOHNSON 2011). In summary, the canonical Hippo cascade is Hippo/Mst → Warts/LATS ⊣ YAP/TAZ+TEAD.

Genetic studies in *Drosophila* and mammalian cells revealed an absolute requirement for Wts/LATS in pathway function, but a partial or context-dependent requirement for Hippo/MST1/2. These observations prompted the discovery of other Ste20-family kinases, but outside the Hippo subfamily, that act redundantly or in parallel to Hippo in specific contexts (MENG *et al.* 2015; ZHENG *et al.* 2015), highlighting the complexity of inputs upstream of Wts/LATS. In most metazoans, the Hippo pathway maintains tissue homeostasis by allowing organs to expand or regress in response to developmental or environmental cues, and its dysregulation contributes to tumorigenesis. Upstream kinases and scaffolds act as tumor suppressors, while YAP/TAZ and TEAD can serve as oncogenic drivers when overactivated (MOROISHI *et al.* 2015; PEARSON *et al.* 2021; HAN *et al.* 2024; HARVEY AND TANG 2025).

A distinctive feature of the Hippo pathway that distinguishes it from other pathways is the absence of a conventional extracellular signaling ligand and transmembrane receptor. Instead, the upstream Hippo kinase is activated by diverse structural elements of the cell: the cytoskeleton, apicobasal cell polarity, and substrate-cell/cell-cell adhesion (MARTIN-BELMONTE AND PEREZ-MORENO 2011). Attenuation of these structures accompany epithelial-to-mesenchymal transition, and hence activation of YAP/TAZ signaling is a major driver of tumor progression (KAPOOR *et al.* 2014; LIN *et al.* 2023). Triggering of downstream YAP activity also suppresses anoikis (FRISCH *et al.* 2013).

Yet in the nematode worm *Caenorhabditis elegans*, development is largely invariant and mosaic: most cell fates are determined by lineage rather than by cell-cell signaling. This rigid developmental program underlies its consistent organ size and stereotyped embryogenesis, unlike the plastic growth observed in flies or vertebrates (HARIHARAN 2015; ROTHMAN AND JARRIAULT 2019). Consequently, canonical Hippo phenotypes – tissue overgrowth or undergrowth – have not been observed in *C. elegans*, and conventional forward genetic screens have not recovered mutants in Hippo, Warts, YAP, or TEAD.

98 Nonetheless, molecular conservation suggested that a core Warts→YAP/TEAD module might be present.
99 Warts is conserved as WTS-1, whose loss causes early larval arrest with compromised intestinal integrity
100 under nutrient stress (CAI *et al.* 2009; KANG *et al.* 2009). YAP-1 and the TEAD ortholog EGL-44 physically
101 interact and are negatively regulated by WTS-1 (IWASA *et al.* 2013), and WTS-1-dependent arrest
102 requires both YAP-1 and EGL-44 (LEE *et al.* 2019). Similarly, NFM-1, the ortholog of Merlin/NF2, the well-
103 established co-regulator of Wts in *Drosophila* and a tumor suppressor in mammals, acts in parallel to
104 WTS-1 to support intestinal polarity and developmental progression (LEE *et al.* 2019). Together, these
105 findings suggest that while the molecular framework of WTS-1→YAP-1/EGL-44 is conserved, it does not
106 drive proliferative phenotypes as in other metazoans.
107 In *C. elegans,* the role of the namesake Hippo kinase in *C. elegans* remains unclear. Two nearly
108 identical Ste20-family kinases, CST-1 and CST-2, share homology with Hippo but differ at the C-terminus:
109 CST-2 lacks three exons encoding the canonical SARAH coiled-coil domain, a motif characteristic of
110 Hippo, Salvador, and RASSF proteins that mediates homo- and -hetero-dimerization and pathway
111 activation (KARCHUGINA *et al.* 2021). RNAi depletion of both genes induces autophagy and affects aging
112 (LEHTINEN *et al.* 2006; WILKINSON *et al.* 2015), and double deletion causes mild neural defects but no
113 arrest, with no clear connection to the WTS-1→YAP-1/EGL-44 axis. These findings have led to the
114 proposal that *C. elegans* lacks Hippo input to WTS-1 (YANG AND HATA 2013).
115 This background raises a central question: does *C. elegans* employ Hippo-related kinases to activate
116 WTS-1 repression of YAP-1, or has regulation of the pathway diverged from canonical mechanisms? To
117 address this, we developed a fluorescent YAP-1 reporter to directly monitor pathway activity and assess
118 the contributions of CST-1/2 and other Ste20 kinases to WTS-1 regulation in two distinct tissues. We
119 validated this tool by showing that WTS-1 cell autonomously represses YAP-1 in both epithelium and
120 intestine. In the epithelium, Hippo-like proteins CST-1/2, like WTS-1, repress YAP-1, indicating likely
121 conservation of the canonical Hippo signaling pathway. In contrast, in the intestine repression of YAP-1
122 upstream of WTS-1 may occur independently of or in parallel to CST-1/2. These findings highlight both
123 the conservation and divergence of Hippo signaling mechanisms in *C. elegans*.
124

125 **RESULTS**

126 **WTS-1 is required for larval development and represses YAP-1 and EGL-44/TEAD to promote**
127 **developmental progression.** A prior study reported that the *wts-1(ok753)* deletion allele causes early
128 larval arrest (KANG *et al.* 2009). To more comprehensively characterize the terminal phenotype and
129 expand available genetic tools, we analyzed two additional alleles: *wts-1(tm4081)*, a deletion not
130 available during the original study, and *wts-1(re436)*, a gene disruption (see below). We also developed
131 a conditional depletion strategy using an auxin-inducible degron (AID*) to acutely remove endogenous
132 WTS-1 protein (**Fig. S1A**).

133 As expected, animals homozygous for *wts-1(ok753)* or *wts-1(tm4081)* exhibited early larval arrest.
134 Both alleles were outcrossed and rebalanced with a fluorescently tagged *tmC18* balancer (DEJIMA *et al.*
135 2018) covering the *wts-1* locus on Chromosome I. Homozygotes segregated from heterozygous mothers
136 arrested at the L2 stage (**Fig. 1A,B**; **S1A**). Arrested animals continued to move and pump for several
137 days, indicating they were alive (**Fig. 1C**). Differential interference contrast (DIC) microscopy revealed
138 no overt structural defects in L2-arrested animals of either genotype. However, both locomotion and
139 pumping declined by Day 3, suggesting reduced physiological health. This finding is consistent with
140 earlier observations of loss of intestinal integrity and cytoskeletal disorganization in *wts-1(ok753)* animals
141 subjected to prolonged starvation (KANG *et al.* 2009). We speculate that sustained WTS-1 loss
142 compromises animal resilience, perhaps including intestinal integrity. This differs from arrest caused by
143 loss of the small GTPase RHEB-1 or mTORC1, where animals remain viable and can live a full *C. elegans*
144 lifespan after hatching (DUONG *et al.* 2020).

145 Knockout consortium mutants are heavily mutagenized and can harbor background mutations. SO
146 using CRISPR/Cas9-dependent genome editing, we introduced a STOP-IN cassette (WANG *et al.* 2018)
147 into the 5' end of the *wts-1* locus to generate *wts-1(re436)*, a 43 bp insertion that also removes the A of
148 the ATG start codon (**Fig. S1A**). While *wts-1(re436)* mutants arrested, many progressed beyond L2,
149 suggesting that this allele is not a complete loss-of-function (**Fig. 1B**). To assess residual gene activity,
150 we compared *wts-1(re436)* and *wts-1(ok753)* animals grown on *control(RNAi)* versus *wts-1(RNAi)*. *wts-*
151 *1(ok753)* animals showed mildly enhanced arrest on *wts-1(RNAi)*, with some animals arresting in L1 (**Fig.**
152 **S1B**), likely due to depletion of maternally contributed gene product. These results suggest that *wts-*
153 *1(ok753)* is a strong loss-of-function allele, and that a full null phenotype may manifest as L1 or L1/L2
154 arrest. *wts-1(re436)* animals exhibited a more severe phenotype when exposed to *wts-1(RNAi)* than to
155 *control(RNAi)*, confirming that *re436* mutants retain partial function. As *wts-1* has an 81 nt 5′ UTR,
156 transcriptional initiation is likely unaffected by *re346*. We speculate that the mutant transcript may
157 undergo cryptic translation initiation downstream of the disrupted ATG.

158 To enable conditional chemical-genetic depletion of endogenous WTS-1, we used CRISPR/Cas9 to
159 insert an *mTurquoise2::2xMyc::AID** tag at the 5′ end of the *wts-1* coding sequence, using the same guide
160 RNA as the STOP-IN strategy (mTurquois2, or mT2, is a blue fluorescent protein). This minimal AID*
161 degron (44 amino acids) is recognized by the TIR1 E3 ubiquitin ligase, which mediates degradation of
162 AID*-tagged proteins in the presence of auxin (indole-3-acetic acid; IAA; (ZHANG *et al.* 2015). The
163 insertion was determined to be error-free by Sanger sequencing. However, we were unable to visualize
164 blue-tagged WTS-1 beyond very faint signal from the intestinal brush border and we have struggled to
165 detect Myc tags in our lab (Wu and Reiner, unpublished results).

166 AID*::WTS-1+somatic TIR1 embryos hatched on auxin plates showed delayed development relative
167 to vehicle-treated controls at Day 3. However, by Day 4, these animals had still reached adulthood,

168 indicating developmental delay rather than arrest (**Fig. 1D–I**), indicating depletion was incomplete. In
169 contrast, double depletion with both auxin treatment and *wts-1(RNAi)* caused robust L2 arrest at both
170 Day 3 and Day 4, closely resembling the phenotype of strong loss-of-function alleles (**Fig. 1D, J–N**).
171 Expression of TIR1 in the germline did not confer arrest in auxin-treated AID*::WTS-1 animals (**Fig. S1C**),
172 suggesting that WTS-1 is not essential for embryonic development prior to the maternal-to-zygotic
173 transition in gene expression. Additionally, animals expressing somatic TIR1 but lacking the AID* tag
174 developed normally in the presence of auxin (**Fig. S1D–F**), confirming that auxin itself does not impair
175 development.
176
177 **WTS-1 is required to repress YAP-1 and EGL-44/TEAD for development progression past beyond**
178 **L2.** Previous work by Lee and colleagues demonstrated that the *wts-1* mutant arrest depends on the
179 activity of YAP-1 and the TEAD transcription factor EGL-44 (LEE *et al.* 2019). This observation is
180 consistent with the conserved role of Warts/LATS kinases in repressing YAP/TAZ and TEAD in *Drosophila*
181 and mammals (*i.e.* Hippo/Mst → Warts/LATS ⊣ YAP/TAZ+TEAD) (HANSEN *et al.* 2015; DASGUPTA AND
182 MCCOLLUM 2019). We tested whether RNAi directed against *yap-1* or *egl-44* could suppress the L2 arrest
183 of *wts-1(tm4081)* animals. *yap-1(RNAi)* fully reversed while *egl-44(RNAi)* partially reversed the arrest
184 (**Fig. 1O**). Similarly, both *yap-1(RNAi)* and *egl-44(RNAi)* suppressed the developmental delay caused by
185 auxin treatment in AID*::WTS-1 animals (**Fig. S1G–J**). These results corroborate the findings of Lee *et*
186 *al.* using new genetic alleles and validate the use of conditional WTS-1 depletion. We conclude that WTS-
187 1 represses YAP-1 and EGL-44/TEAD to permit developmental progression, a mechanism that is
188 conserved among metazoans.
189
190 **Generation of tagged endogenous YAP-1 for use as a reporter of upstream signaling.** The
191 transcriptional coactivator *Drosophila* Yorkie (Yki) and its human orthologs Yap and TAZ are well
192 established reporters of upstream Wts/LATS activity. Their subcellular localization reflects regulation by
193 upstream kinases, particularly the Warts serine/threonine kinase (LATS1/2 in mammals). In this
194 conserved mechanism, phosphorylation of YAP by Warts prevents nuclear entry by promoting
195 cytoplasmic retention; inactivation of Warts permits dephosphorylation and nuclear translocation of YAP
196 (HANSEN *et al.* 2015; DASGUPTA AND MCCOLLUM 2019).
197 Hata and colleagues (IWASA *et al.* 2013) identified the *C. elegans* ortholog of YAP-1 and generated a
198 high-copy integrated translational reporter (*yap-1*p>*yap-1::gfp*). GFP expression from this transgene is
199 broad and YAP-1::GFP signal is predominantly cytoplasmic, with pronounced nuclear exclusion,
200 particularly in epithelial tissues. WTS-1 and the 14-3-3 protein FTT-2 are predicted inhibitors of YAP-1
201 nuclear localization (HANSEN *et al.* 2015; DASGUPTA AND MCCOLLUM 2019). Consistent with this
202 prediction, RNAi-mediated depletion of *wts-1* or *ftt*-2 resulted in nuclear accumulation of YAP-1::GFP,

203 supporting an evolutionarily conserved role for Warts-mediated inhibition of YAP in *C. elegans* (IWASA *et*
204 *al.* 2013).
205 In contrast, RNAi of other putative upstream components failed to cause nuclear accumulation of
206 YAP-1::GFP. These negative results include depletion of *cst-1* and *cst-2*, which encode predicted Hippo-
207 like kinases resembling mammalian MST1/2, the eponymous initiators of the pathway. These negative
208 results raise doubts that the Hippo pathway is conserved in *C. elegans* upstream of Warts and Yap (IWASA
209 *et al.* 2013). Indeed, the "Hippo pathway" in *C. elegans* has been debated as to whether it is a conserved
210 signaling module, a collection of disconnected components, or ignored in the discussion altogether
211 (HALDER AND JOHNSON 2011; YANG AND HATA 2013). Similar ambiguity surrounds the *C. elegans*
212 "Hedgehog" pathway, which retains a GLI transcription factor ortholog but lacks most core pathway
213 elements, but in the case of Hedgehog the conclusion is the pathway has been mostly lost during
214 evolution (BURGLIN AND KUWABARA 2006).
215 We reasoned that the high expression level of transgenic YAP-1::GFP may reduce sensitivity to
216 perturbation of upstream signal. Possible explanations include buffering of phosphorylation due to
217 excessive protein levels, a lower signal-to-noise ratio in detection of fluorescence, insufficient RNAi
218 knockdown to overcome the threshold required for YAP-1 nuclear entry, or potential redundancy of the
219 duplicated *cst-1* and *cst-2* genes (though these duplicated genes are mostly identical at the DNA level,
220 see below).
221 To generate a more sensitive and physiologically relevant reporter of endogenous YAP-1 dynamics,
222 we used CRISPR/Cas9-dependent genome editing to insert sequences encoding a short linker,
223 mNeonGreen (a photostable, yellow-shifted fluorescent protein; (SHANER *et al.* 2013) and a 2x FLAG
224 epitope at the 3' end of the *yap-1* coding sequence, generating *yap-1(re269[yap-1::mNG::2xflag])*; **Fig.**
225 **S2A**). The resulting edited *yap-1* was error-free by Sanger sequencing. Immunoblotting with anti-FLAG
226 antibody confirmed the predicted tagged protein size of 80.6 kDA (**Fig. S2B**). YAP-1::mNG::2xFLAG was
227 crossed with blue-fluorescent histone marker HIS-72::mT2 and imaged, revealing apparently ubiquitous
228 expression relative to the wild type and low background autofluorescence from unedited controls.
229 Representative images of epithelium and intestine are shown (**Fig. S2C**).
230
231 **WTS-1 represses YAP-1 nuclear translocation in epithelium and intestine.** In all systems studied to
232 date, Warts/LATS1/2 kinases repress YAP nuclear translocation. To test whether this regulatory
233 mechanism is conserved in *C. elegans*, we used our endogenously tagged YAP-1::mNG reporter to
234 monitor subcellular localization in response to WTS-1 depletion.
235 We constructed a reporter strain expressing YAP-1::mNG (yellow, imaged at 514 nm) and HIS-
236 72::mTurquoise2 (blue, imaged at 445 nm) for nuclear reference. This strain also harbored a *rrf-3* loss-

237 of-function mutation to enhance sensitivity to RNAi (SIMMER *et al.* 2002). Despite this sensitization, *wts-*
238 *1(RNAi)* did not cause overt developmental delay or lethality in this strain.
239 However, imaging revealed that *wts-1(RNAi)* robustly induced nuclear accumulation of YAP-1::mNG
240 in both epithelial cells (**Fig. 2A-C**) and intestinal cells (**Fig. 2D-F**), compared to *control(RNAi)*. These
241 results were recapitulated using the AID*::WTS-1 system: addition of auxin induced nuclear translocation
242 of YAP-1::mNG in epithelial (**Fig. S2D-F**) and intestinal cells (**Fig. S2G-I**), relative to vehicle-treated
243 controls.
244 Unexpectedly, we found that the mNG::2xFLAG knock-in into the C-terminus of YAP-1 suppressed
245 the lethality associated with *wts-1* deletion. Double mutants of genotype *wts-1(tm4081)*; *yap-1(re269[yap-*
246 *1::mNG::2xflag])* developed normally, showing no arrest or delay, and were fully viable and fertile (**Fig.**
247 **S2J-L**), in stark contrast to *wts-1* single mutants (**Fig. 1**). Nevertheless, YAP-1::mNG strongly
248 accumulated in the nucleus in both epithelial and intestinal cells of *wts-1(tm4081)* mutants (**Fig. S2M-P'**).
249 Lee *et al*. had showed that *wts-1(RNAi)* in an *rrf-3* mutant background conferred arrest, but the
250 endogenous *yap-1* gene in their experiment was unaltered (KANG *et al.* 2009).
251 Notably, a previous study used an exogenous *yap-1*p>*yap-1::gfp* transgene (IWASA *et al.* 2013), which
252 would not reveal defects in co-transcriptional activity caused by C-terminal tagging. Yet this defect was
253 unexpected, as key functional domains of YAP-1, including the TEAD binding domain (TBD) and WW
254 domains, are located at the N-terminus and central region of the protein, respectively, across diverse
255 species (HILMAN AND GAT 2011; YANG AND HATA 2013; MESROUZE *et al.* 2021).
256 We conclude that YAP-1::mNG is a reliable reporter of upstream WTS-1 activity, with nuclear
257 localization reflecting loss of WTS-1-mediated inhibition. However, the C-terminally tagged YAP-1::mNG
258 does not appear to function as a transcriptional coactivator; while some YAP/TAZ proteins have a C-
259 terminal PDZ-recognition motif, these are not present in insect YAP proteins nor in YAP-1 (HILMAN AND
260 GAT 2011). Since *yap-1* deletion mutants are superficially wild type (LEE *et al.* 2019; APKEN AND
261 OECKINGHAUS 2021), the transcriptional defect caused by C-terminal tagging of YAP-1 would remain
262 unnoticed unless assayed in a *wts-1* mutant background, where L2 arrest is reversed by loss of YAP-1
263 function.
264
265 **WTS-1 functions cell autonomously to repress YAP-1 in epithelium and intestine.** A key test for of
266 cell-cell signaling function is cell autonomy: does a protein function in the tissue manifesting the mutant
267 phenotype or another tissue? Previous results showed that the early larval arrest of *wts-1(ok753)* animals
268 was rescued by transgenic expression of *wts-1(+)* expressed by an intestinal promoter, demonstrating
269 that intestinal expression of WTS-1 is sufficient to support development (KANG *et al.* 2009). Using our
270 conditional chemical-genetic degron, we used tissue-specific expression of the cofactor for AID*-auxin to

271 test the converse question: in which tissue is WTS-1 necessary to support normal developmental
272 progression?
273 We expressed TIR1, the E3 ubiquitin ligase substrate recognition protein for AID*, specifically in
274 intestinal or epithelial tissues and treated AID*::WTS-1 with auxin vs. vehicle as described (ASHLEY *et al.*
275 2021). In AID*::WTS-1 animals expressing epithelial TIR1 and grown on *wts-1(RNAi)* to increase
276 robustness, addition of auxin caused mild growth delay relative to vehicle controls (**Fig. 3A-C**). The same
277 outcome occurred without RNAi, though with reduced severity (**Fig. S3A-C**). Degradation efficacy was
278 monitored using degradation of a tissue-specific AID*-tagged nuclear BFP reporter as an internal control.
279 In epithelial TIR1 animals not treated with *wts-1(RNAi)*, auxin induced BFP degradation and nuclear
280 accumulation of YAP-1::mNG in the epithelium (**Fig. 3G-I'**), but not in the intestine (**Fig. 3I-J'**).
281 In the converse experiment, intestinal TIR1 expression with auxin treatment in *wts-1(RNAi)* animals
282 caused complete developmental arrest (**Fig. 3D-F**), with weaker effects without RNAi (**Fig. S3D-F**). Auxin
283 treatment also induced intestinal BFP degradation and nuclear translocation of YAP-1::mNG in the
284 intestine, but not in the epithelium (**Fig. 3K-L", I-J"**).
285 These results confirm tissue-specific degradation via the AID*-TIR1 system and show that WTS-1 is
286 required in the intestine for developmental progression and repression of YAP-1::mNG. This
287 complements prior rescue studies of *wts-1(Δ)* with intestinally driven *wts-1(+)* (KANG *et al.* 2009). We also
288 find that WTS-1 represses YAP-1::mNG in epithelium, and that epithelial WTS-1 depletion causes a
289 modest growth delay, though whether this is related to intestinal effects remains unclear.
290
291 **CST-1/2, the putative *C. elegans* Hippo ortholog, represses YAP-1::mNG in epithelium but not**
292 **intestine.** In *Drosophila* and mammals, Hippo (Hpo) and MST1/2 are Ste20-family kinases (DAN *et al.*
293 2001; DELPIRE 2009) that regulate growth via activation of Wts and hence repression of YAP/TEAD. While
294 conserved in many species, a clear Hippo ortholog function in *C. elegans* had not been established.
295 *C. elegans* encodes two Hippo-like kinases, CST-1 and CST-2, are roughly equivalently expressed
296 from tandemly duplicated genes on chromosome X (**Fig. 4A**; mean FPKM of 32 and 24 for *cst-1* and *cst-*
297 *2*, respectively). These proteins are 100% identical through most of their sequence, including the kinase
298 domain, but differ in the final 13 amino acids of exon 9. *cst*-2 CDS (coding DNA sequence) stops at the
299 end of exon 9, while *cst-1* contains three additional exons that are not present in *cst-2*. Importantly, CST-
300 2 lacks the C-terminal SARAH coiled-coil domain present in all Hpo-related proteins, including CST-1
301 (**Fig. S4A**), which is essential in other systems for Hippo signaling via homo- and hetero-dimerization
302 (KARCHUGINA *et al.* 2021). Thus, CST-2 may be regulated differently, act independently, or be a non-
303 functional byproduct of genomic duplication.
304 100% DNA identity extends through all shared exons and upstream sequences of *cst-1* and *cst-2*,
305 even extending several hundred bp upstream of the ATG initiator methionine codon (**Fig. S4B,C**).

306 Examined related Caenorhabditid nematodes encode only a single CST-1 ortholog with a SARAH
307 domain, suggesting a recent duplication event in *C. elegans*.
308 The *cst-1-cst-*2 genomic region was previously deleted as a validation of the transposon-mediated
309 MosDEL deletion technology (FROKJAER-JENSEN *et al.* 2010). In our hands, mutants for the resulting
310 lesion, *basDf1*, are viable, grow slightly slowly, and defective for locomotion. We deleted the *cst-1/2* locus
311 – from exon 1 of *cst-2* to intron 11 of *cst-1* – using CRISPR/Cas9-dependent genome editing, creating
312 the *cst-1/2(reDf4[re452])* allele (**Fig. 4A**). Deletion of *cst-1/2*, like *basDf1*, conferred slow growth and mild
313 locomotion defects, but was not arrested.
314 The absence of lethality from Δ*cst-1/2* mutants, in contrast to Δ*wts-1*, leads us to speculate that CST-
315 1/2 does not recapitulate the role of WTS-1 throughout the animal. Yet in the *reDf4* mutant, YAP-1::mNG
316 translocated to epithelial nuclei (**Fig. 4B-D**), similar to WTS-1 depletion, suggesting CST-1 and possibly
317 CST-2 activate WTS-1 in epithelium.
318 Strikingly, *Δcst-1/2* did not cause nuclear YAP-1::mNG translocation in intestine (**Fig. 4E-G**). Given
319 that intestinal *wts-1(+)* rescues *wts-1(ok753)* and that intestinal WTS-1 degradation causes arrest, we
320 propose that CST-1/2 is not necessary for the intestinal WTS-1-dependent event, only the epithelial WTS-
321 1-dependent event. This observation is consistent with studies in flies and mammals, where in certain
322 contexts Hippo/Mst1/2 mutants showed less penetrant phenotypes than Warts/LATS mutants, likely due
323 to kinase redundancy at the level of Ste20 family kinases Hippo/Mst1/2 (MENG *et al.* 2015; ZHENG *et al.*
324 2015).
325
326 **Deletion/depletion of both CST-1/2 and Ste20-family kinase MIG-15 cause WTS-1-like L2 arrest.**
327 Previous studies identified Ste20-family kinases from the GCK-I and GCK-IV subfamilies functioning
328 redundantly with Hippo/MST1/2 to activate Wts/LATS1/2 in flies and mammalian cells (MENG *et al.* 2015;
329 ZHENG *et al.* 2015). Specifically, these are the GCK-I and GCK-IV subfamilies of the Ste20 family (DAN
330 *et al.* 2001; DELPIRE 2009). Both consist of N-terminal Ste20 kinase domains and C-terminal CNH (Citron
331 homology) domains, yet they are distinct subfamilies in metazoans. The GCK-I subfamily includes *C.*
332 *elegans* GCK-2*,* fly Happyhour, and mammalian MAP4K1,2,3,5. The GCK-IV subfamily includes *C.*
333 *elegans* MIG-15*,* fly Misshapen, and mammalian MAP4K4,6,7,8. We previously showed that in *C.*
334 *elegans* GCK-2 promotes vulval 2° fate and MIG-15 promotes vulval 3° fate (SHIN *et al.* 2018; FAKIEH
335 AND REINER 2025).
336 We tested whether these Ste-20-family GCK-I and GCK-IV subfamily kinases function redundantly
337 with CST-1/2 to activate WTS-1. In AID*::mNG::2xHA::MIG-15 animals with somatic TIR1, auxin
338 treatment of MIG-15-depleted animals caused mild growth delay (**Fig. 5A-D, I-J**). With same experiment
339 in a *cst-1/2(Δ)* background, auxin-induced MIG-15 depletion caused robust L2 arrest, phenocopying *wts-*
340 *1* mutants (**Fig. 5E-H, I-J**). Also, as with deficient *wts-1*, MIG-15 and CST-1/2 deficient and arrested

341 animals continued movement and feeding (**Fig. 5K**). This arrest phenotype was reversed by *yap-1(RNAi)*
342 and to a lesser extent by *egl-44(RNAi)* (**Fig. 5L-O**). One interpretation is that MIG-15 also contributes to
343 WTS-1/YAP-1 regulation. Alternatively, the function of MIG-15 could be entirely in parallel to CST-1/2;
344 RNAi of *yap-1* or *egl-44* may suppress effects of mutant *cst-1/2* to retore growth, without impacting the
345 downstream consequences of mutant *mig-15*.
346 To test the Ste20-family GCK-I subfamily member GCK-2, we generated animals with *cst-1/2(Δ)*,
347 AID*::MIG-15, and somatically expressed TIR1 with and without *gck-2(re483)*. Animals arrested upon
348 addition of auxin regardless of whether *gck-2* was deleted (**Fig. S5A-J**). Triple mutant *gck-2 cst-1/2 mig-*
349 *15* animals continued feeding (**Fig. S5K**), like *cst-1/2 mig-15* mutants or *wts-1* mutants, above. A STOP-
350 IN allele, *gck-2(re427)*, edited into the *cst-1/2(Δ)* YAP-1::mNG animal, failed to send YAP-1::mNG into
351 the nucleus (**Fig. 5SL-O**). Thus, GCK-2 does not appear to contribute to this developmental event, though
352 we cannot rule out GCK-2 in other Hippo-regulated signaling events in the animal.
353
354 **Ste20-family kinase MIG-15 represses YAP-1::mNG levels but not nuclear translocation.** Given the
355 synthetic L2 arrest in auxin+AID*::MIG-15-depleted *cst-1/2(Δ)* animals, we examined YAP-1::mNG
356 localization in these backgrounds. Our MIG-15 tag thus far is with sequences encoding mNeonGreen
357 (FAKIEH AND REINER 2025), which would interfere with visualization of YAP-1::mNG nuclear translocation.
358 Consequently, we used CRISPR/Cas9-dependent genome editing to insert mTurquoise2::2xMyc::AID*
359 at the 5' end of *mig-15* in animals expressing somatic TIR1 and YAP-1::mNG (**Fig. S6A**). MIG-15
360 depletion by auxin caused a protruding-vulva phenotype found in all *mig-15* mutants (**Fig. S6B-C**),
361 consistent with strong depletion.
362 Surprisingly, auxin+AID*::MIG-15 depletion with *cst-1/2(+)*increased total YAP-1::mNG levels but did
363 not induce nuclear localization. In epithelial cells, we observed perinuclear aggregation of YAP-1::mNG
364 (**Fig. 6A-C**), potentially indicating localization to Golgi. In intestine, MIG-15 depletion increased YAP-
365 1::mNG expression and weak nuclear localization, but less than that observed in *wts-1* (**Fig. 6D-G**).
366 We expected that combined MIG-15 depletion and *cst-1/2(Δ)* would cause robust YAP-1::mNG
367 nuclear localization. Instead, nuclear levels resembled those in MIG-15 depletion alone (**Fig. 6H-K**).
368 While this result was unexpected, the synthetic L2 arrest and rescue by *yap-1(RNAi)* and *egl-44(RNAi)*
369 suggest that MIG-15 and CST-1/2 converge on WTS-1 or YAP-1 regulation. However, they may regulate
370 YAP-1 via different mechanisms or in parallel pathways, as shown in our model of these results (**Fig. 7**).
371
372
373 **DISCUSSION**
374 In this study, we established that *C. elegans* epithelium possesses the molecular wiring of a canonical
375 Hippo→Warts ⊣ YAP/TEAD pathway, while also revealing unexpected divergence in its tissue-specific

regulation, specific in intestine. Using an endogenous YAP-1 fluorescent reporter, we showed that WTS-1 cell-autonomously excludes YAP-1 from the nucleus in both epithelia and intestine. Tissue-specific depletion of WTS-1 demonstrated that WTS-1 cell-autonomously prevents animal arrest in intestine. At the same time, our data show that the upstream Hippo-related kinases CST-1/2 contribute to YAP-1 regulation only in the epithelium, while intestinal regulation proceeds through a distinct, CST-1/2-independent or CST-1/2-parallel mechanism. We identified MIG-15, the nematode ortholog of *Drosophila* Msn and mammalian MAP4K4,6,7,8 kinases – implicated in activation of fly and mammalian Wts/LATS in parallel to Hippo/MST1/2 – as redundant with CST-1/2 developmental progression past the L2 stage and reliant on inhibition of YAP-1/EGL-44. Unexpectedly, MIG-15 represses of abundance of YAP-1 protein, perhaps through blocking a degradative process, but not nuclear translocation. Together, these results establish a hybrid picture: a canonical Hippo-like cascade in the epithelium *vs.* noncanonical, parallel inputs to WTS-1 in the intestine.

Divergence of Hippo inputs in *C. elegans*. The presence of one Hippo kinase with a canonical SARAH-domain (CST-1) and another Hippo kinase without (CST-2), coupled with the redundant CST-1/2 kinases not being essential like WTS-1, has fueled uncertainty about whether a *bona fide* Hippo pathway operates in *C. elegans*. Our findings clarify this issue. CST-1/2 act as functional Hippo-like inputs in the epithelium, supporting the model of conservation of the canonical cascade. However, in intestine regulation appears to rely on unknown, alternate kinases. In flies and mammals, MAP4K family members (orthologous to GCK-2 and MIG-15 in worms) act redundantly with Hippo to activate LATS/WTS (MENG *et al.* 2015; ZHENG *et al.* 2015). Our analysis shows that MIG-15, but not GCK-2, alters YAP-1 protein levels in nematodes, suggesting that these kinases may have retained ancillary regulatory functions while losing the ability to control YAP-1 nuclear localization. This divergence highlights the evolutionary plasticity of Hippo inputs across cell types.

Alternatively, MIG-15 and GCK-2 may contribute to phosphorylation of WTS-1 and repression of YAP-1 in other tissues. Epithelium and intestine were assayed because they are large tissues with nuclei readily imaged via confocal microscopy during development. Yet many other tissues or individual cells undergo myriad developmental events while forming the mature animal. For example, EGL-44 regulates identity of a small set of neurons (WU *et al.* 2001), but we would not know if deficiency of WTS-1 or CST-1/2 impacted nuclear translocation of YAP-1 during a key developmental window in the life of these neurons.

Functional outcomes without proliferation. A striking feature of the *C. elegans* Hippo pathway is the absence of proliferative mutant phenotypes. In other animals, Hippo signaling governs tissue size, regeneration, and tumorigenesis; in nematodes, cell lineages and organ sizes, and indeed animal size,

411 is mostly fixed. Our findings suggest that while the molecular wiring is conserved, the transcriptional
412 outputs of YAP-1/EGL-44 may have shifted. Many YAP/TEAD target genes in *C. elegans* are linked to
413 pathogen responses and gut barrier integrity (MA *et al.* 2020). We hypothesize that YAP-1/EGL-44 has
414 been uncoupled from growth-control genes – either through changes in regulatory DNA elements or
415 altered DNA-binding specificity of EGL-44 – and thus repurposed to support stress and barrier functions.
416 In this sense, *C. elegans* provides a model for Hippo signaling stripped of its growth-control role,
417 emphasizing instead its contributions to tissue robustness.
418
419 **Interpreting the arrest phenotype**
420 Loss of WTS-1 causes developmental arrest accompanied by defective intestinal integrity. This arrest
421 could reflect the requirement of an EGL-44/TEAD target gene expression for developmental progression,
422 while other genes are required for tissue integrity. Alternatively, perhaps arrest is a secondary
423 consequence of developmental defects, say perhaps a developmental checkpoint in response to loss of
424 gut integrity, or an intestinal defect that results in starvation. Analogies may be drawn to the mTORC1
425 pathway, where stress of reduced anabolism can cause programmed diapause at a variety of stages
426 (DUONG *et al.* 2020; SUN *et al.* 2025). Unexpectedly, hyperactivation of YAP-1/EGL-44 upon loss of WTS-
427 1 reduces, rather than enhances, robustness of gut integrity. This finding contrasts with the presumed
428 protective induction of YAP/TEAD in response to pathogenesis/barrier disruption (MA *et al.* 2020),
429 suggesting a feedback loop in which excessive pathway activity destabilizes epithelial function. As with
430 Hippo-mediated growth in other systems, balanced homeostasis may be critical in the gut.
431
432 **Tissue- and process-specific roles.** Our work complements previous studies showing that RNAi
433 depletion of *cst-1/2* induces autophagy and influences lifespan (LEHTINEN *et al.* 2006; WILKINSON *et al.*
434 2015), phenotypes not easily explained through WTS-1 or YAP-1. Similarly, Hippo-related roles in
435 neuronal development have been reported in *C. elegans*, unattached to WTS-1 or YAP-1/EGL-44 (FENG
436 *et al.* 2017; JOSEPHSON *et al.* 2017; LEE *et al.* 2018). While our WTS-1 null animals did not exhibit
437 locomotion defects, *cst-1/2* deletions were Uncoordinated and slightly undergrown, suggesting that CST-
438 1/2 may act independently of WTS-1 in sculpting the nervous system. Future experiments will be needed
439 to determine whether YAP-1 or EGL-44 contribute to these locomotory phenotypes.
440
441 **Contributions of this work.** Our results extend prior studies in several important ways. First, we used a
442 novel endogenous YAP-1 reporter to directly monitor Hippo activity *in vivo*, validating WTS-1-dependent
443 repression across two tissues. Second, we employed tissue-specific depletion strategies to show that
444 WTS-1 regulation is cell-autonomous. Third, we clarified the contributions of CST-1/2, identifying them
445 as functional Hippo-like kinases in the epithelium but perhaps not intestine. Finally, we assessed functions

446 of Ste20-family orthologs, showing that GCK-2 does not contribute to YAP-1 regulation while MIG-15
447 influences YAP-1 stability but not localization. Together, these analyses position *C. elegans* as a unique
448 model in which Hippo signaling is preserved at the level of WTS-1 inhibition of YAP-1 but diverges in its
449 upstream regulation and biological outputs.
450
451 **Broader implications.** The field of Hippo signaling has been dominated by studies of over-proliferation,
452 regeneration and tumorigenesis. *C. elegans* provides a contrasting model in which conserved pathway
453 components are retained but uncoupled from growth control. Instead, Hippo signaling contributes to
454 epithelial robustness, stress responses, and possibly neural development. These findings underscore the
455 evolutionary flexibility of Hippo signaling and open new directions for understanding how signaling
456 pathways are rewired to meet the developmental logic of different organisms.
457
458
459 **METHODS**
460 ***C. elegans* handling and genetics.** All *C. elegans* strains were derived from the N2 Bristol wild type and
461 grown on NG agar plates seeded with the OP50 strain *E. coli* at 20˚C unless otherwise noted. Growth,
462 culturing and nomenclature were generally as described (BRENNER 1974; HORVITZ *et al.* 1979; TULI *et al.*
463 2018). Wormbase was used extensively during these studies (STERNBERG *et al.* 2024).
464
465 **CRISPR/Cas9 mediated genome editing.** Guide RNAs were that maximally satisfied a combination of
466 three approaches. First, where possible, G and not T nucleotides were selected at positions -1/-2, or
467 GCGG and not T-TT nucleotides at positions -1/-2/-3/-4 (KAPOOR *et al.* 2014; FARBOUD AND MEYER 2015).
468 Second, we considered strong predicted specificity and efficiency scores using the CRISPOR
469 (http://crispor.tefor.net/) algorithm, which incorporates the original MIT specificity score. Third, we
470 considered strong predicted efficiency scores using the WU-CRISPR (http://crisprdb.org/wu-crispr/)
471 algorithm.
472 We formulated mixes for microinjection as described previously (FAKIEH *et al.* 2022). Using a
473 dedicated RNase-free bench, we mixed concentrations as final volume per 20 μL: 1 μl of 5 μg/μl stock
474 *Streptococcus pyogenes* Cas9 (PNAbio, #CP01) for 0.25 μg/μl final concentration; 1μl of 2 μg/μl stock
475 universal tracrRNA (IDT) for 0.1 μg/μl final concentration; 1.4 μl each of 0.4 μg/μl stocks of *dpy-10* co-
476 CRISPR and gene-specific crRNAs for 0.028 μg/μl crRNA final concentration each. Not yet at final
477 volume, this mix was incubated at 37°C for 15 min. After incubation, *dpy-10* ssODN repair oligo was
478 added as 3.3 μl of 20 μM stock for final concentration of 3.3 μM; gene-specific column-purified PCR repair
479 template was denatured and renatured as described (GHANTA AND MELLO 2020), and added from stock
480 of ≤300 ng/μl to a final concentration of 100 ng/μl (total final concentration of PCR product no greater

481 than 2 µg/20 µl for reasons of viscosity). As this point, commercial nuclease-free water was added up to
482 20 µl. (Concentrations before the incubation were calculated per 20 µl, but 20 µl volume was not reached
483 until the final addition of water.)
484 Adult animals with no more than a single row of embryos in each uterus side were microinjected as
485 described (KADANDALE *et al.* 2009). We used co-CRISPR to generate dominant Rol mutations in F1
486 animals harboring the *dpy-10(cn64*gf*)* marker (ARRIBERE *et al.* 2014), which were picked singly or in pools
487 of two to plates. After F1 Rols had laid embryos, the single or pooled parents were picked to PCR tubes,
488 lysed for PCR and detected via triplex PCR. Non-Dpy/Rol F2s were picked singly, incubated overnight to
489 obtain genetic material, lysed and PCR detected to generate homozygous lines. Knockins were
490 sequenced from points in flanking DNA outside that subjected to homology-directed recombination repair.
491 Only expected knockins were used for analysis.
492
493 **RNA interference.** Plates for bacterially mediated RNAi interference (RNAi) were made with NGM agar
494 supplemented with 1 mM IPTG and 50 µg/mL carbenicillin. Plates were spotted with 80 µl of HT115
495 bacteria culture expressing dsRNA as described (TIMMONS *et al.* 2001). L4 P0s were picked to 24 hr-
496 seeded RNAi plates, grown overnight, then transferred the next day to fresh RNAi plates for synchronized
497 laying of embryos. The P0s were removed 24 hours later and F1 animals were analyzed at the time
498 appropriate for the experiments. Positive control for efficacy of RNAi plates was *pop-1(RNAi),* where we
499 expect 95-100% embryonic or L1 lethality of the experiment is discarded. For negative control with used
500 *luciferase(RNAi)* as previously described (SHIN *et al.* 2018), to engage the RNAi machinery with a
501 sequence not encoded in the *C. elegans* genome. RNAi was performed at 20˚C.
502
503 **Pumping assays.** Benchtop mechanical clickers were uses to count contractions of the pharynx
504 ("pumping") per 60 sec. Observations used a Nikon SMZ18 stereo microscope.
505
506 **Auxin treatment.** Auxin (IAA; Indole-3-acetic acid, 98+%, Thermo Scientific) storage stock solution was
507 prepared at 400 mM in ethanol and stored up to a month at 4˚C. For experiments, stock auxin was diluted
508 to 16 mM working auxin stock by diluting storage 400 mM auxin with filtered Milli-Q water. For final
509 concentration of 1 mM auxin in plates, 500 µl of 16 mM auxin was added onto 8 ml NGM agar plates or
510 RNAi plates and allowed to diffuse. For vehicle control, 500 µl of 4% ethanol was similarly added to
511 plates.
512
513 **Detection of tagged endogenous YAP-1::mNG::2xFLAG.** Mixed-stage animals were washed from 3-
514 4 full but not starved plates using M9 buffer and lysed in 4% SDS loading buffer with boiling at 90˚C for
515 2 min. Samples were run on a 4-15% SDS-PAGE gel (Bio-Rad, #5671084) and transferred to Immobilon-

516 P Membrane, PVDF (EMD Millipore, IPVH00010). Mouse monoclonal anti-Flag antibody (Sigma-Aldrich,
517 F1804) and mouse monoclonal anti-α-tubulin antibody (Sigma-Aldrich, T6199) were diluted 1:2000 in
518 blocking solution (6% w/v non-fat dry milk in PBST). HRP conjugated goat anti-mouse secondary
519 antibody (Sigma-Aldrich, 12-349) was diluted 1:5000 in blocking solution. Chemiluminescent detection
520 was performed using ECL reaction (Thermo Fisher Scientific 32106) and detected via film processor,
521 SRX-101A (Konica Minolta) on X-ray film (Phenix).
522
523 **Imaging.** Animals used for live imaging were mounted on a 5% agar pad on a glass slide in 5 μl of 2
524 mg/ml tetramisole in M9 buffer with cover slip. Confocal microscopy used a Nikon Ti2 microscope with a
525 Yokogawa CSU-W1 Spinning Disk, 405 nm, 445 nm, 514 nm lasers, and a Photometrics Prime BSI
526 camera, and NIS Elements Advanced Research software, version 5.42. Quantification of fluorescence
527 intensity were performed by ImageJ (Fiji) with a customized script code (deposited at:
528 https://github.com/ReidTPowell/2025_Genetics_Reiner). In 3-channel confocal
529 photomicrographs analyzed in ImageJ with the script running, the user identifies the center of a
530 nucleus in the DIC channel and placed a point using the "multi-point tool." The script draws a
531 uniform circle for each point of interest and measures fluorescence intensity. This confers
532 precision in area of circle from sample to sample.
533 10 cm NG plate photomicrographs were captured using a Nikon Eclipse Ni microscope, 4x objective,
534 ANDOR Zyla sCMOS camera and NIS Elements Advanced Research software, version 4.30, with plate
535 and animals on the stage with sufficient working distance.
536
537 **Sequence analysis.** Protein sequences were accessed via Wormbase (wormbase.org; (STERNBERG *et*
538 *al.* 2024) and Alliance of Genome Resources (https://www.alliancegenome.org/). We used the A isoform
539 for both *cst-1* and *cst-2*, thus excluding the two-codon minority splice addition to exon 9 for both. *mig-15*
540 isoform A was selected as the reference and most abundant isoform. Uniprot accession numbers were
541 Q13188 for human MST1/STK3, Q13043 for human MST2/STK4, Q8T0S6 for *Drosophila* Hpo. Protein
542 sequences were aligned with Clustal Omega (https://www.ebi.ac.uk/jdispatcher/msa/).
543
544 **Statistical analysis.** Animal experiments presented in the same graph were scored concurrently.
545 Statistical analyses were performed by two-tail unpaired Student's t-test or Fisher's Exact test (GraphPad
546 Prism 10).
547
548 **Software/website**
549 GraphPad Prism was used for statistical analysis and making graphs. BioRender
550 (https://www.biorender.com/) was used to generate illustrations. Exon-Intron Graphic Maker was used for

551 making schematic gene structures http://wormweb.org/exonintron. AI software was used only for text
552 editing purposes.
553
554 **Data availability statement.**
555 Strains, plasmids and sequence files are available upon request. All data supporting the conclusions of
556 the study and required for reproduction of experiments are present within the text, tables and figures.
557
558 **Conflicts of interest.**
559 None.
560
561 **Acknowledgements.** We thank L. Vergara in the Center for Advanced Imaging for technical assistance,
562 members of the Reiner lab for helpful discussions and technical expertise, J. Bembenek (Wayne State
563 University) for the strain harboring HIS-72::mT2, M. Bastiani (University of Utah) for *basDf1*, Y. Hata
564 (Tokyo Medical and Dental University) and B. Grant (Rutgers University) for the strain harboring
565 *ihIs35[yap-1*p*>yap-1::GFP], and* S. Mitani (Japanese National Bioresource Project) for *wts-1(tm4081)*.
566 Some strains were provided by the *Caenorhabditis* Genetics Center, which is funded by the NIH Office
567 of Research Infrastructure Programs (P40 OD010440). Wormbase was used extensively. Our CRISPR
568 protocol was based on an amalgam protocol generously shared by Dr. Andy Golden (NIDDK).
569
570 **Funding**. This work was funded by NIH grants R35GM144237 and R03CA289854 to D.J.R.
571
572
573
574 **Supplementary Tables.**
575 Strains used are shown in Table S1.
576 Oligonucleotides in Table S2.
577 Guide RNAs in Table S3.
578 Plasmids in Table S4.
579
580 **Figure Legends**
581 **Figure 1. Loss of WTS-1 confers YAP-1/YAP and EGL-44/TEAD-dependent developmental arrest.**
582 **(A)** Schematic of experimental design for scoring *wts-1* mutant developmental stages. **(B)** Quantification
583 of arrest stages of homozygous *wts-1* mutant compared to the heterozygote on Day 3. △1 = *wts-*
584 *1(tm4081).* △2 = *wts-1(ok753).* * = *wts-1(re436[STOP-IN*]). **(C)** Pumping rate/60s of *wts-1(tm4081)*
585 homozygote vs. heterozygote. (**D)** Schematic of protocol for auxin treatment of **E-H)** *wts-*

586 *1(re419[mTurq2::2xMyc::AID*::wts-1])*; *ieSi57[eft-3p::TIR1::mRuby]* animals grown on vehicle or 1 mM
587 auxin, scored on Day 3 or Day 4. **I)** Quantification of developmental stage for animals in **E-H**. **(J-M)** The
588 same animals as above grown on vehicle or 1 mM auxin and *ctrl(RNAi)* vs *wts-1(RNAi)*, scored on Day
589 3 or Day 4. *ctrl(RNAi)* = luciferase sequences with no homology in the *C. elegans* genome (Shin *et al.*
590 2018). **(N)** Quantification of developmental stage for animals in **J-M**. **(O)** Quantification of developmental
591 stages on Day 3 of *wts-1(tm4081)* treated with *ctrl(RNAi)*, *yap-1(RNAi)* or *egl-44(RNAi)*. ****=P<0.0001,
592 ***=P<0.001, **=P<0.01, ns = not significant (Fisher's exact test).
593
594 **Figure 2: YAP-1::mNG functions as a reporter for WTS-1 activity in epithelium and intestine. (A-C)**
595 Confocal and DIC photomicrographs and quantification of lateral epithelium; animals are oriented side-
596 up. Animal genotype is *rrf-3(re390[STOP-IN])*; *his-72(erb77[his-72::linker::mTurquoise2])*; *yap-*
597 *1(re269[yap-1::mNG::2xflag])* to confer hypersensitivity to RNAi. **(A-B")** Cytoplasm-to-nuclear
598 translocation of endogenous YAP-1::mNG grown on *ctrl(RNAi)* vs. *wts-1(RNAi)* bacteria, respectively. **(C)**
599 Quantification of fluorescence intensity in **A-B"** of nuclear YAP-1::mNG in arbitrary units (A.U.). N =
600 multiple nuclei from 9 and 10 animals, respectively. **(D-F)** Confocal and DIC photomicrographs and
601 quantification of intestine, left-right mid-animal plane; animals are oriented side-up. Animals are depicted
602 at lower magnification to show multiple intestinal nuclei. **(D-E")** Cytoplasm-to-nuclear translocation of
603 endogenous YAP-1::mNG grown on *ctrl(RNAi)* vs. *wts-1(RNAi)* bacteria. Animal genotype is *rrf-*
604 *3(re390[STOP-IN])*; *his-72(erb77[his-72::linker::mTurquoise2])*; *yap-1(re269[yap-1::mNG::2xflag])* to
605 confer hypersensitivity to RNAi. **(F)** Quantification of fluorescence intensity in **D-E"** of nuclear YAP-
606 1::mNG as A.U.. N = multiple nuclei from 4 and 5 animals, respectively. Epithelium scale bars = 20 µm,
607 pop out scale bars for intestine = 10 µm. **** = P<0.0001 (*t*-test).
608
609 **Figure 3. Effects of tissue-specific depletion of AID*::WTS-1. (A,B)** Bright field photomicrographs of
610 animals with AID*::WTS-1 depletion: global RNAi with epithelial-specific AID* depletion via epithelial-
611 specific expression of TIR1. Genotype is *wts-1(re419[mT2::2xMyc::AID*::wts-1]); reSi2[col-*
612 *10p>TIR1::F2A::mTagBFP2::AID::NLS::tbb-2 3'UTR]*. **(A)** Animals grown on vehicle+*ctrl(RNAi) vs.* **(B)**
613 auxin+*wts-1(RNAi)*. **(C)** Quantification of **(A** vs. **B)**. **(D,E)** Bright field photomicrographs of animals
614 AID*::WTS-1 depletion: global RNAi with intestinal-specific AID* depletion via intestinal-specific
615 expression of TIR1. Genotype is *wts-1(re419[mT2::2xMyc::AID*::wts-1])*; *reSi12[ges-*
616 *1p>TIR1::F2A::mTagBFP2::AID::NLS::tbb-2 3'UTR]*. **(D)** Animals grown on vehicle+*ctrl(RNAi) vs.* **(E)**
617 auxin+*wts-1(RNAi)*. **(F)** Quantification of **(D** vs. **E)**. Scale bars = 1 mm. ****=P<0.0001 (Fisher's exact
618 test). **(G-N')** Effects on YAP-1::mNG localization of depletion of WTS-1 in epithelium vs. intestine. **(G-J')**
619 Confocal and DIC photomicrographs of epithelium (**G-G",I-I"**) vs. intestine (**H-H',J-J'**) with YAP-1::mNG,
620 epithelial-specific TIR1+AID*::BFP and AID*::WTS-1, no RNAi. Genotype is *wts-*

621 *1(re419[mT2::2xMyc::AID*::wts-1])*; *reSi2[col-10p>TIR1::F2A::mTagBFP2::AI*D::NLS::tbb-2 3'UTR]*;
622 *yap-1(re269[yap-1::mNG::2xFlag])*. **(G-H')** vehicle-treated animal vs. **(I-J')** auxin-treated. **(G'** vs. **I')** Note
623 auxin-dependent depletion of nuclear BFP internal control in epithelium. **(K-N')** Confocal and DIC
624 photomicrographs of intestine (**K-K'',M-M''**) vs epithelium (**L-L',N-N'**) with YAP-1::mNG, intestinal-
625 specific TIR1+AID*::BFP and AID*::WTS-1, no RNAi. Genotype is *wts-1(re419[mT2::2xMyc::AID*::wts-*
626 *1])*; *reSi12[ges-1p>TIR1::F2A::mTagBFP2::AID*::NLS::tbb-2 3'UTR]*; *yap-1(re269[yap-1::mNG::2xFlag])*.
627 **(K-L')** vehicle-treated animal vs. **(M-N')** auxin-treated. **(K'** vs. **M')** Note auxin-dependent depletion o
628 nuclear BFP internal control in intestine. Scale bars in epithelial confocal images: 20 µm. Scale bars in
629 intestinal confocal images = 10 µm.
630
631 **Figure 4: The CST-1/2 putative Hippo orthologs inhibit YAP-1::mNG in epithelium but not intestine.**
632 **(A)** Schematic of *cst-1* and *cst-2* genomic region on Chromosome X. The red line indicates the
633 *reDf4[re452]* deletion, which removes *cst-1*, *cst-2* and seven ncRNA genes in between. Lines above the
634 chromosome map indicate conserved protein domains from protein products. CST-2 lacks the C-terminal
635 SARAH (Sav/RASSF/Hpo) coiled-coiled dimerization domain present in the C-terminus of *cst-1* and
636 Hippo proteins in other metazoans. **(B-D)** Confocal photomicrographs, DIC photomicrographs and
637 quantification of lateral epithelium (animals are oriented side-up). Animal genotypes are *i.e.* wild type vs.
638 *cst-1/2* deletion: *his-72(erb77[his-72::linker::mT2])*; *yap-1(re269[yap-1::mNG::2xflag]) vs. his-*
639 *72(erb77[his-72::linker::mT2])*; *cst-1/2(reDf4[re452]) yap-1(re269[yap-1::mNG::2xflag]).* **D)** Quantification
640 of fluorescence intensity in **B-C''** of nuclear YAP-1::mNG in arbitrary units (A.U.). N = multiple nuclei from
641 9 and 10 animals, respectively. **(E-G)** Confocal photomicrographs, DIC photomicrographs, and
642 quantification of intestine, left-right mid-animal intestinal plane (animals are oriented side-up). Animals
643 are depicted at lower magnification to show multiple intestinal nuclei. Animal genotypes are *his-*
644 *72(erb77[his-72::linker::mT2])*; *yap-1(re269[yap-1::mNG::2xflag]) vs. his-72(erb77[his-72::linker::mT2])*;
645 *cst-1/2(reDf4[re452]) yap-1(re269[yap-1::mNG::2xflag])*, *i.e.* wild type vs. *cst-1/2* deletion. N = multiple
646 nuclei from 4 animals each. Epithelium scale bars = 20 µm, pop out scale bars = 10 µm. ****=P<0.0001,
647 ns = not significant (*t*-test)
648
649 **Figure 5. CST-1/2 functions redundantly with MIG-15 to control developmental progression. (A-**
650 **H)** Bright-field photomicrographs of depleted AID*::MIG-15 with or without deleted *cst-1/2*, scored on day
651 3 (**A,B,E,F**) and day 4 (**C,D,G,H**) to illustrate degree of growth delay/arrest. Genotypes are *ieSi57[eft-*
652 *3p>TIR1::mRuby::unc-54 3'UTR + Cbr-unc-119(+)]; unc-119(ed3); mig-15(re264[AID*::mNG::2xHA::mig-*
653 *15])* (**A-D**)*vs. ieSi57[eft-3p>TIR1::mRuby::unc-54 3'UTR + Cbr-unc-119(+)]*; *unc-119(ed3)*; *mig-*
654 *15(re264[AID*::mNG::2x::mig-15]) cst-1/2(reDf1[re484])* (**E-H**). (**B,D** and **F,H**) Treatment with 1 mM auxin
655 *vs.* vehicle on other plates. Depletion of *AID*::MIG-15* causes mild growth delay and locomotion defects

656 (**A/C** vs **B/D**), as published for *mig-15* mutants. Deletion of *cst-1/2* causes mild growth delay and
657 locomotion defects (**A/C** vs **E/G**), as we observed on plates mutant for *basDf1* or *cst-1/2(reDf1[re484])*
658 **(I,J)** Quantification of arrest at Day 3 and Day 4, respectively, reveals the strong arrest of *cst-1/2 mig-15*
659 double mutants relative to single mutants. Animal assays shown in (**E,F,G,H**) and their quantification in
660 (**I,J**), in columns with N of 143 and 135, respectively, are recapitulated in **Fig. S5**, to contrast the effects
661 with and without mutant *gck-2*. All were scored concurrently. **(K)** Pumping rate of control *vs.* double
662 mutant on Day 1 and Day 3 indicates arrest, not lethality. N=10 animals for each group. Animals also
663 continue to swim. **(L-N)** Growth arrest phenotype of AID*::MIG-15 depletion combined with *cst-1/2*
664 deletion was reversed by *yap-1(RNAi)* or *egl-44(RNAi)*. **(O)** quantification of **L-N**. ****=P<0.0001,
665 ***=P<0.001, **=P<0.01, ns= not significant. Scale bar = 1 mm.
666
667 **Figure 6. MIG-15 represses YAP-1 levels but does not restrict nuclear translocation. (A-B')**
668 Confocal and DIC photomicrographs of YAP-1::mNG in lateral epithelium. Animal genotype is *ieSi57[eft-*
669 *3p>TIR1::mRuby::unc-54 3'UTR + Cbr-unc-119(+)]; unc-119(ed3)*; *mig-*
670 *15(re435[mT2::2xMyc::AID*::mig-15) yap-1(re269[yap-1::mNG::2xflag])* on vehicle *vs.* auxin,
671 respectively. **(C)** Quantification of YAP-1::mNG intensity in AID*::MIG-15 animals with and without auxin.
672 N = multiple nuclei from 10 and 9 animals, respectively. **(D-E')** Confocal and confocal photomicrographs
673 of YAP-1 in midline intestine. Animal genotype is *ieSi57[eft-3p>TIR1::mRuby::unc-54 3'UTR + Cbr-unc-*
674 *119(+)]; unc-119(ed3)*; *mig-15(re435[mT2::2xMyc::AID*::mig-15) yap-1(re269[yap-1::mNG::2xflag])* on
675 vehicle vs. auxin. Fluorescence intensity was measured for nucleus **(F')** and cytoplasm **(G')**, respectively.
676 N = multiple nuclei from 9, 10 animals, respectively.**(H-J')** Confocal and confocal photomicrographs of
677 YAP-1 in midline intestine. Animal genotype is *ieSi57[eft-3p::TIR1::mRuby::unc-54 3'UTR + Cbr-unc-*
678 *119(+)]; unc-119(ed3)*; *mig-15(re435[mT2::2xMyc::AID*::mig-15) yap-1(re269[yap-1::mNG::2xflag]) cst-*
679 *1/2(re479)* on vehicle vs. auxin. Fluorescence intensity was measured for nucleus **(H')** and cytoplasm
680 (**I**'), respectively. N=10-18 animals. Scale bars = 10 µm. ****=P<0.0001, ***=P<0.001. (*t*-test)
681
682 **Figure 7. A model for Hippo and Warts signaling in *C. elegans*. (A)** In epithelium a canonical Hippo
683 pathway functions, with potentially redundant CST-1 and CST-2 phosphorylating and activating WTS-1.
684 WTS-1 in turn phosphorylates and inhibits YAP-1, keeping it out of the nucleus. Disruption of CST-1/2 or
685 WTS-1 results in nuclear translocation of YAP-1, as observed in other systems. Rather than contributing
686 to activation of WTS-1 to repress YAP-1, MIG-15 inhibits YAP-1 protein levels. **(B)** In Intestine a non-
687 canonical Hippo pathway functions. Unknown upstream inputs regulate WTS-1 to phosphorylate and
688 retain YAP-1 out of the nucleus. Loss of WTS-1 causes nuclear translocation of YAP-1 but also L2 arrest,
689 indicated as "Growth." CST-1/2 and MIG-15 act redundantly to maintain growth.
690

691

692 **REFERENCES**

693 Apken, L. H., and A. Oeckinghaus, 2021 The RAL signaling network: Cancer and beyond. Int Rev Cell
694 Mol Biol 361: 21-105.
695 Arribere, J. A., R. T. Bell, B. X. Fu, K. L. Artiles, P. S. Hartman *et al.*, 2014 Efficient marker-free recovery
696 of custom genetic modifications with CRISPR/Cas9 in Caenorhabditis elegans. Genetics 198:
697 837-846.
698 Ashley, G. E., T. Duong, M. T. Levenson, M. A. Q. Martinez, L. C. Johnson *et al.*, 2021 An expanded
699 auxin-inducible degron toolkit for Caenorhabditis elegans. Genetics 217.
700 Brenner, S., 1974 The genetics of Caenorhabditis elegans. Genetics 77: 71-94.
701 Burglin, T. R., and P. E. Kuwabara, 2006 Homologs of the Hh signalling network in C. elegans.
702 WormBook: 1-14.
703 Cai, Q., W. Wang, Y. Gao, Y. Yang, Z. Zhu *et al.*, 2009 Ce-wts-1 plays important roles in Caenorhabditis
704 elegans development. FEBS Lett 583: 3158-3164.
705 Dan, I., N. M. Watanabe and A. Kusumi, 2001 The Ste20 group kinases as regulators of MAP kinase
706 cascades. Trends Cell Biol 11: 220-230.
707 Dasgupta, I., and D. McCollum, 2019 Control of cellular responses to mechanical cues through YAP/TAZ
708 regulation. J Biol Chem 294: 17693-17706.
709 Dejima, K., S. Hori, S. Iwata, Y. Suehiro, S. Yoshina *et al.*, 2018 An Aneuploidy-Free and Structurally
710 Defined Balancer Chromosome Toolkit for Caenorhabditis elegans. Cell Rep 22: 232-241.
711 Delpire, E., 2009 The mammalian family of sterile 20p-like protein kinases. Pflugers Arch 458: 953-967.
712 Duong, T., N. R. Rasmussen, E. Ballato, F. S. Mote and D. J. Reiner, 2020 The Rheb-TORC1 signaling
713 axis functions as a developmental checkpoint. Development 147.
714 Fakieh, R., T. Duong, Y. Wu, N. Rasmussen and D. Reiner, 2022 A simple strategy for addition of degron
715 tags to endogenous genes harboring prior insertions of fluorescent protein. MicroPubl Biol 2022.
716 Fakieh, R. A., and D. J. Reiner, 2025 RAP-2 and CNH-MAP4 Kinase MIG-15 confer resistance in
717 bystander epithelium to cell-fate transformation by excess Ras or Notch activity. Proc Natl Acad
718 Sci U S A 122: e2414321121.
719 Farboud, B., and B. J. Meyer, 2015 Dramatic enhancement of genome editing by CRISPR/Cas9 through
720 improved guide RNA design. Genetics 199: 959-971.
721 Feng, G., Z. Zhu, W. J. Li, Q. Lin, Y. Chai *et al.*, 2017 Hippo kinases maintain polarity during directional
722 cell migration in Caenorhabditis elegans. EMBO J 36: 334-345.
723 Frisch, S. M., M. Schaller and B. Cieply, 2013 Mechanisms that link the oncogenic epithelial-
724 mesenchymal transition to suppression of anoikis. J Cell Sci 126: 21-29.
725 Frokjaer-Jensen, C., M. W. Davis, G. Hollopeter, J. Taylor, T. W. Harris *et al.*, 2010 Targeted gene
726 deletions in C. elegans using transposon excision. Nat Methods 7: 451-453.
727 Ghanta, K. S., and C. C. Mello, 2020 Melting dsDNA Donor Molecules Greatly Improves Precision
728 Genome Editing in Caenorhabditis elegans. Genetics 216: 643-650.
729 Halder, G., and R. L. Johnson, 2011 Hippo signaling: growth control and beyond. Development 138: 9-
730 22.
731 Han, H., Z. Huang, C. Xu, G. Seo, J. An *et al.*, 2024 Functional annotation of the Hippo pathway somatic
732 mutations in human cancers. Nat Commun 15: 10106.
733 Hansen, C. G., T. Moroishi and K. L. Guan, 2015 YAP and TAZ: a nexus for Hippo signaling and beyond.
734 Trends Cell Biol 25: 499-513.
735 Hariharan, I. K., 2015 Organ Size Control: Lessons from Drosophila. Dev Cell 34: 255-265.
736 Harvey, K. F., C. M. Pfleger and I. K. Hariharan, 2003 The Drosophila Mst ortholog, hippo, restricts growth
737 and cell proliferation and promotes apoptosis. Cell 114: 457-467.
738 Harvey, K. F., and T. T. Tang, 2025 Targeting the Hippo pathway in cancer. Nat Rev Drug Discov.
739 Hilman, D., and U. Gat, 2011 The evolutionary history of YAP and the hippo/YAP pathway. Mol Biol Evol
740 28: 2403-2417.
741 Horvitz, H. R., S. Brenner, J. Hodgkin and R. K. Herman, 1979 A uniform genetic nomenclature for the
742 nematode Caenorhabditis elegans. Mol Gen Genet 175: 129-133.

743 Huang, J., S. Wu, J. Barrera, K. Matthews and D. Pan, 2005 The Hippo signaling pathway coordinately
744 regulates cell proliferation and apoptosis by inactivating Yorkie, the Drosophila Homolog of YAP.
745 Cell 122: 421-434.
746 Iwasa, H., S. Maimaiti, H. Kuroyanagi, S. Kawano, K. Inami *et al.*, 2013 Yes-associated protein homolog,
747 YAP-1, is involved in the thermotolerance and aging in the nematode Caenorhabditis elegans.
748 Exp Cell Res 319: 931-945.
749 Josephson, M. P., R. Aliani, M. L. Norris, M. E. Ochs, M. Gujar *et al.*, 2017 The Caenorhabditis elegans
750 NF2/Merlin Molecule NFM-1 Nonautonomously Regulates Neuroblast Migration and Interacts
751 Genetically with the Guidance Cue SLT-1/Slit. Genetics 205: 737-748.
752 Justice, R. W., O. Zilian, D. F. Woods, M. Noll and P. J. Bryant, 1995 The Drosophila tumor suppressor
753 gene warts encodes a homolog of human myotonic dystrophy kinase and is required for the
754 control of cell shape and proliferation. Genes Dev 9: 534-546.
755 Kadandale, P., I. Chatterjee and A. Singson, 2009 Germline transformation of Caenorhabditis elegans by
756 injection. Methods Mol Biol 518: 123-133.
757 Kang, J., D. Shin, J. R. Yu and J. Lee, 2009 Lats kinase is involved in the intestinal apical membrane
758 integrity in the nematode Caenorhabditis elegans. Development 136: 2705-2715.
759 Kapoor, A., W. Yao, H. Ying, S. Hua, A. Liewen *et al.*, 2014 Yap1 activation enables bypass of oncogenic
760 Kras addiction in pancreatic cancer. Cell 158: 185-197.
761 Karchugina, S., D. Benton and J. Chernoff, 2021 Regulation of MST complexes and activity via SARAH
762 domain modifications. Biochem Soc Trans 49: 675-683.
763 Lee, H., J. Kang, S. Ahn and J. Lee, 2019 The Hippo Pathway Is Essential for Maintenance of Apicobasal
764 Polarity in the Growing Intestine of Caenorhabditis elegans. Genetics 213: 501-515.
765 Lee, H., J. Kang and J. Lee, 2018 Involvement of YAP-1, the Homolog of Yes-Associated Protein, in the
766 Wnt-Mediated Neuronal Polarization in Caenorhabditis elegans. G3 (Bethesda) 8: 2595-2602.
767 Lehtinen, M. K., Z. Yuan, P. R. Boag, Y. Yang, J. Villen *et al.*, 2006 A conserved MST-FOXO signaling
768 pathway mediates oxidative-stress responses and extends life span. Cell 125: 987-1001.
769 Lin, W. H., L. M. Cooper and P. Z. Anastasiadis, 2023 Cadherins and catenins in cancer: connecting
770 cancer pathways and tumor microenvironment. Front Cell Dev Biol 11: 1137013.
771 Ma, Y. C., Z. S. Yang, L. Q. Ma, R. Shu, C. G. Zou *et al.*, 2020 YAP in epithelium senses gut barrier loss
772 to deploy defenses against pathogens. PLoS Pathog 16: e1008766.
773 Martin-Belmonte, F., and M. Perez-Moreno, 2011 Epithelial cell polarity, stem cells and cancer. Nat Rev
774 Cancer 12: 23-38.
775 Meng, Z., T. Moroishi, V. Mottier-Pavie, S. W. Plouffe, C. G. Hansen *et al.*, 2015 MAP4K family kinases
776 act in parallel to MST1/2 to activate LATS1/2 in the Hippo pathway. Nat Commun 6: 8357.
777 Mesrouze, Y., F. Bokhovchuk, M. Meyerhofer, C. Zimmermann, P. Fontana *et al.*, 2021 Study of the TEAD-
778 binding domain of the YAP protein from animal species. Protein Sci 30: 339-349.
779 Moroishi, T., C. G. Hansen and K. L. Guan, 2015 The emerging roles of YAP and TAZ in cancer. Nat Rev
780 Cancer 15: 73-79.
781 Oh, H., and K. D. Irvine, 2010 Yorkie: the final destination of Hippo signaling. Trends Cell Biol 20: 410-
782 417.
783 Pearson, J. D., K. Huang, M. Pacal, S. R. McCurdy, S. Lu *et al.*, 2021 Binary pan-cancer classes with
784 distinct vulnerabilities defined by pro- or anti-cancer YAP/TEAD activity. Cancer Cell 39: 1115-
785 1134 e1112.
786 Rothman, J., and S. Jarriault, 2019 Developmental Plasticity and Cellular Reprogramming in
787 Caenorhabditis elegans. Genetics 213: 723-757.
788 Shaner, N. C., G. G. Lambert, A. Chammas, Y. Ni, P. J. Cranfill *et al.*, 2013 A bright monomeric green
789 fluorescent protein derived from Branchiostoma lanceolatum. Nat Methods 10: 407-409.
790 Shin, H., R. E. W. Kaplan, T. Duong, R. Fakieh and D. J. Reiner, 2018 Ral Signals through a MAP4
791 Kinase-p38 MAP Kinase Cascade in C. elegans Cell Fate Patterning. Cell Rep 24: 2669-2681
792 e2665.

Simmer, F., M. Tijsterman, S. Parrish, S. P. Koushika, M. L. Nonet *et al.*, 2002 Loss of the putative RNA-directed RNA polymerase RRF-3 makes C. elegans hypersensitive to RNAi. Curr Biol 12: 1317-1319.

Sternberg, P. W., K. Van Auken, Q. Wang, A. Wright, K. Yook *et al.*, 2024 WormBase 2024: status and transitioning to Alliance infrastructure. Genetics 227.

Sun, C. L., C. Xu, O. Itani, E. L. Christensen, H. Vijay *et al.*, 2025 Biased regulation of protein synthesis and hypoxic death by a conditional raptor mutation. Curr Biol 35: 2567-2582 e2565.

Tapon, N., K. F. Harvey, D. W. Bell, D. C. Wahrer, T. A. Schiripo *et al.*, 2002 salvador Promotes both cell cycle exit and apoptosis in Drosophila and is mutated in human cancer cell lines. Cell 110: 467-478.

Timmons, L., D. L. Court and A. Fire, 2001 Ingestion of bacterially expressed dsRNAs can produce specific and potent genetic interference in Caenorhabditis elegans. Gene 263: 103-112.

Tuli, M. A., A. Daul and T. Schedl, 2018 Caenorhabditis nomenclature. WormBook 2018: 1-14.

Vassilev, A., K. J. Kaneko, H. Shu, Y. Zhao and M. L. DePamphilis, 2001 TEAD/TEF transcription factors utilize the activation domain of YAP65, a Src/Yes-associated protein localized in the cytoplasm. Genes Dev 15: 1229-1241.

Wang, H., H. Park, J. Liu and P. W. Sternberg, 2018 An Efficient Genome Editing Strategy To Generate Putative Null Mutants in Caenorhabditis elegans Using CRISPR/Cas9. G3 (Bethesda) 8: 3607-3616.

Wilkinson, D. S., J. S. Jariwala, E. Anderson, K. Mitra, J. Meisenhelder *et al.*, 2015 Phosphorylation of LC3 by the Hippo kinases STK3/STK4 is essential for autophagy. Mol Cell 57: 55-68.

Wu, J., A. Duggan and M. Chalfie, 2001 Inhibition of touch cell fate by egl-44 and egl-46 in C. elegans. Genes Dev 15: 789-802.

Wu, S., J. Huang, J. Dong and D. Pan, 2003 hippo encodes a Ste-20 family protein kinase that restricts cell proliferation and promotes apoptosis in conjunction with salvador and warts. Cell 114: 445-456.

Wu, S., Y. Liu, Y. Zheng, J. Dong and D. Pan, 2008 The TEAD/TEF family protein Scalloped mediates transcriptional output of the Hippo growth-regulatory pathway. Dev Cell 14: 388-398.

Yang, Z., and Y. Hata, 2013 What is the Hippo pathway? Is the Hippo pathway conserved in Caenorhabditis elegans? J Biochem 154: 207-209.

Zhang, L., F. Ren, Q. Zhang, Y. Chen, B. Wang *et al.*, 2008 The TEAD/TEF family of transcription factor Scalloped mediates Hippo signaling in organ size control. Dev Cell 14: 377-387.

Zhang, L., J. D. Ward, Z. Cheng and A. F. Dernburg, 2015 The auxin-inducible degradation (AID) system enables versatile conditional protein depletion in C. elegans. Development 142: 4374-4384.

Zheng, Y., W. Wang, B. Liu, H. Deng, E. Uster *et al.*, 2015 Identification of Happyhour/MAP4K as Alternative Hpo/Mst-like Kinases in the Hippo Kinase Cascade. Dev Cell 34: 642-655.

Huynh Figure 1

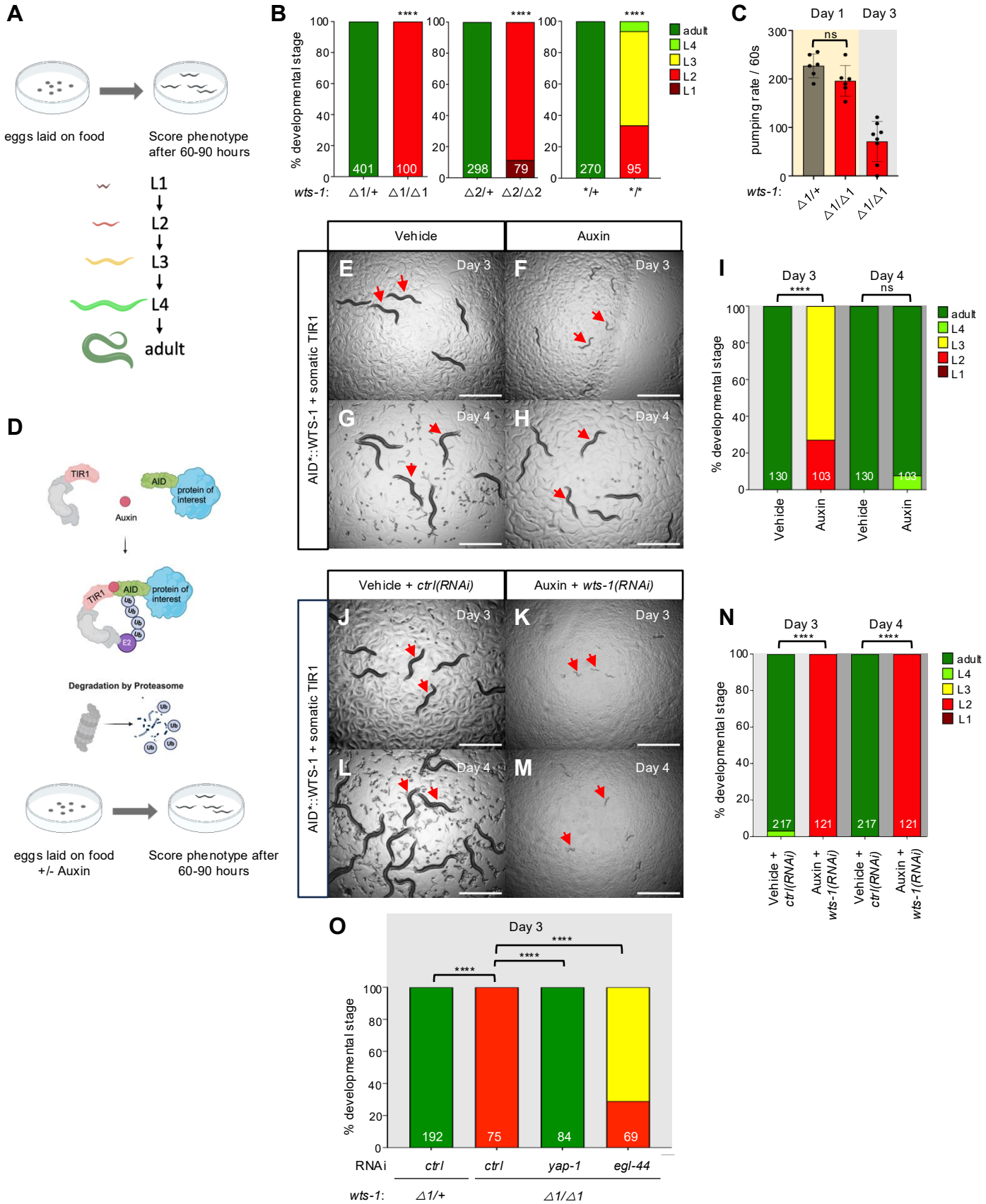

Huynh Figure 2

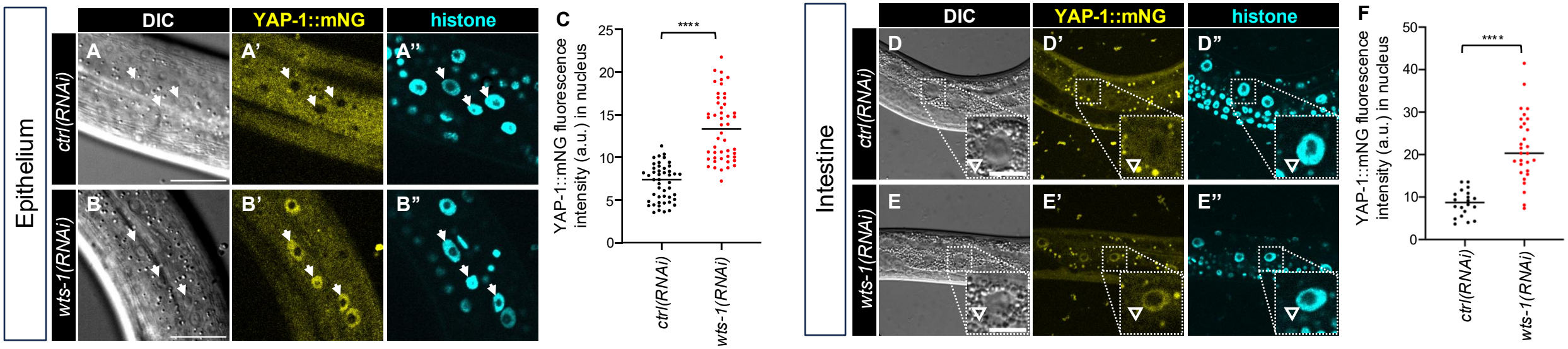

Huynh Figure 3

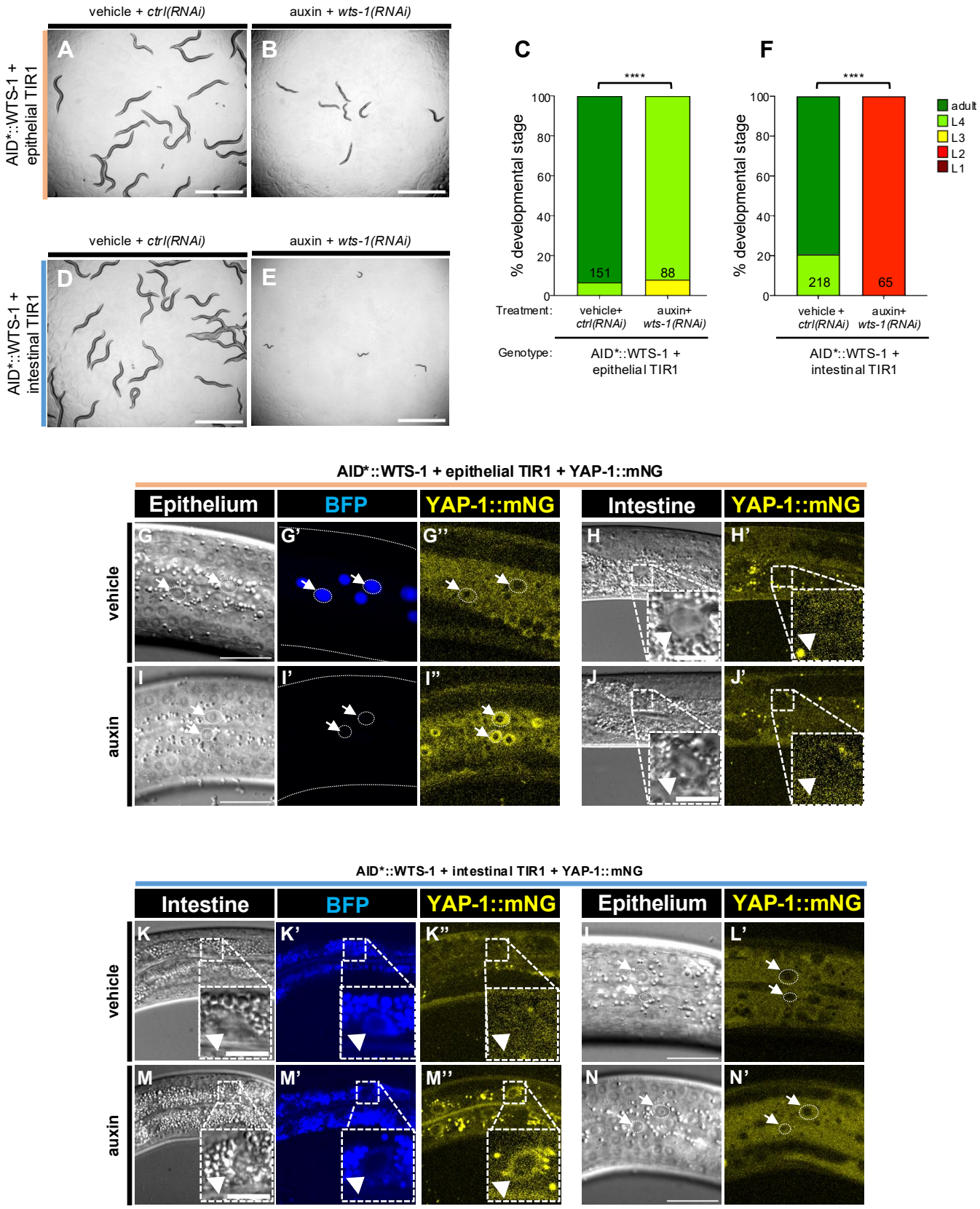

Huynh Figure 4

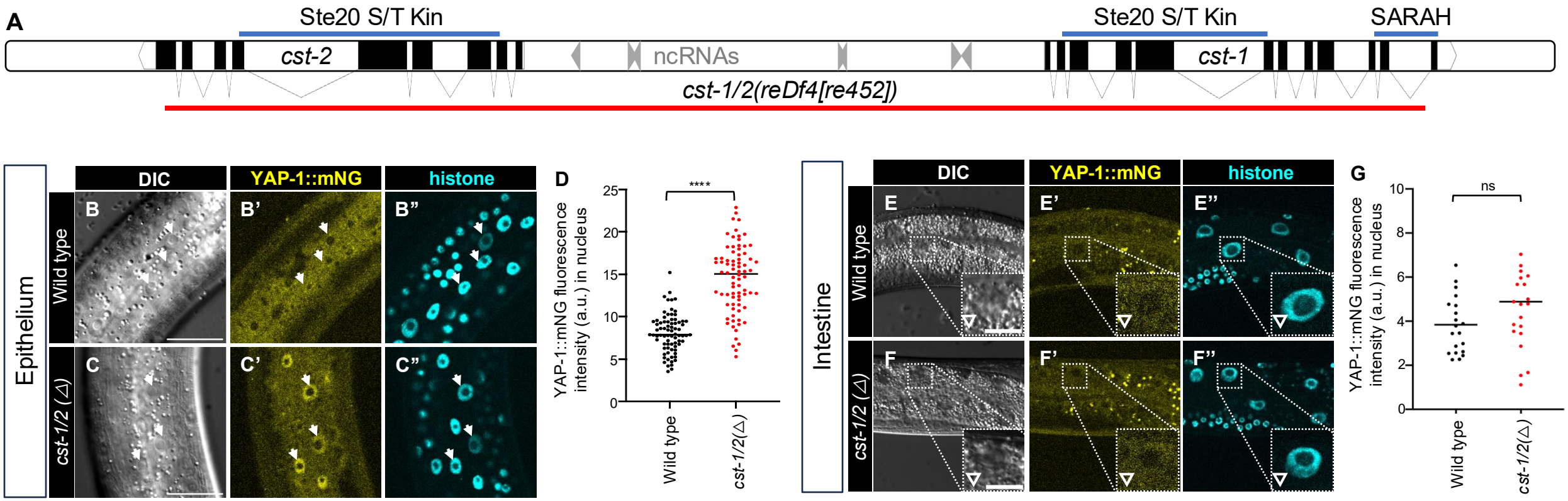

Huynh Figure 5

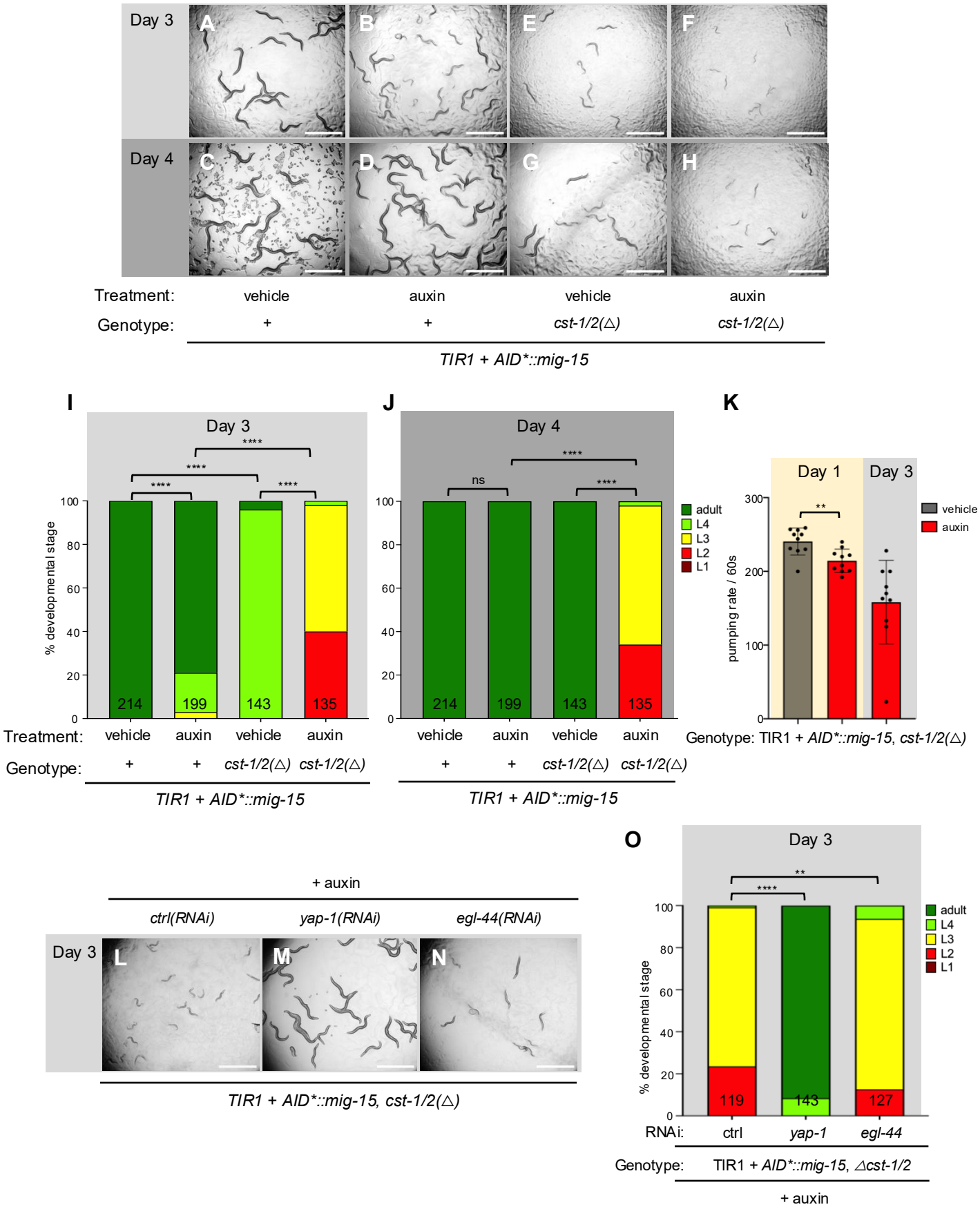

Huynh Figure 6

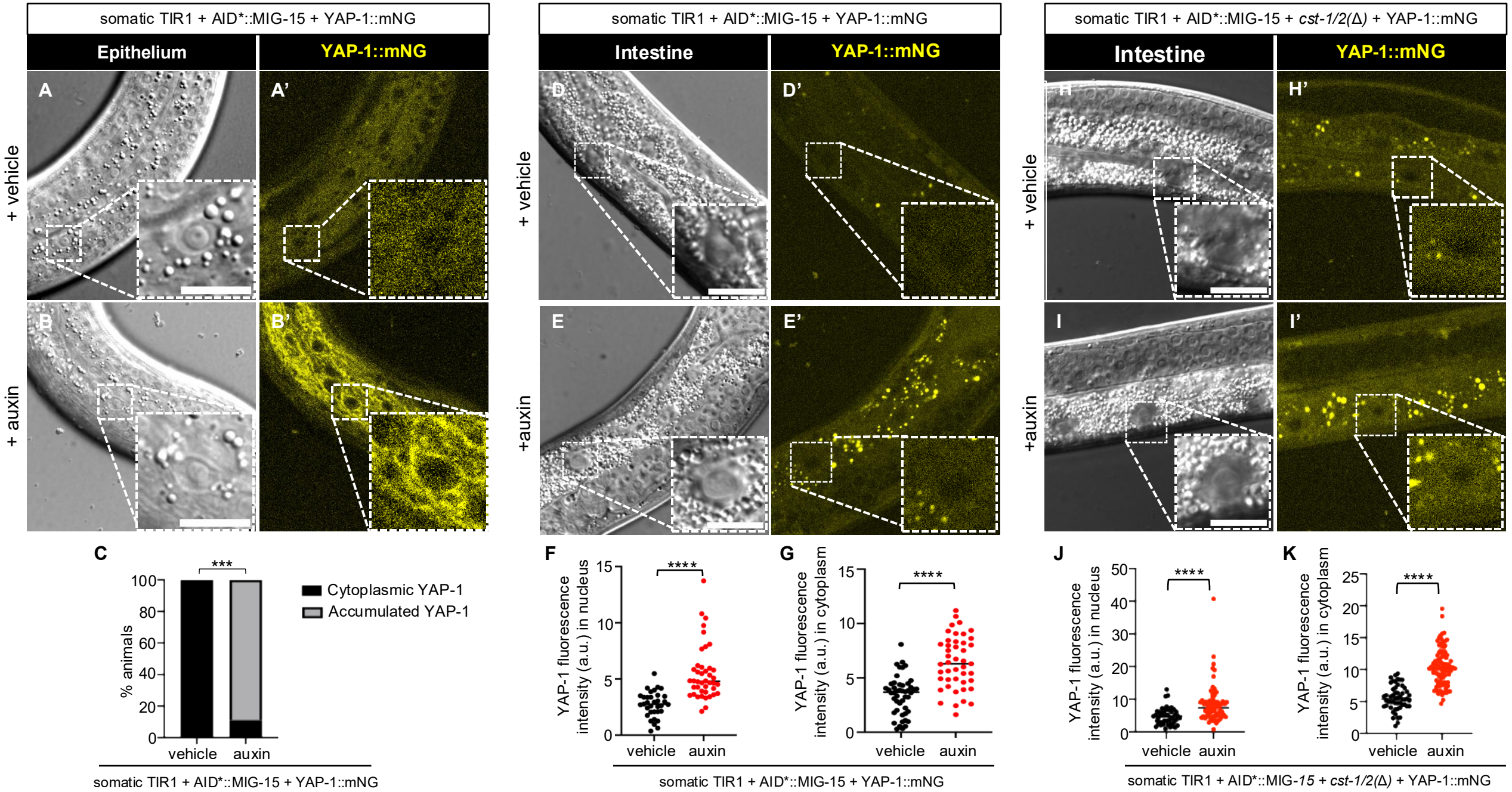
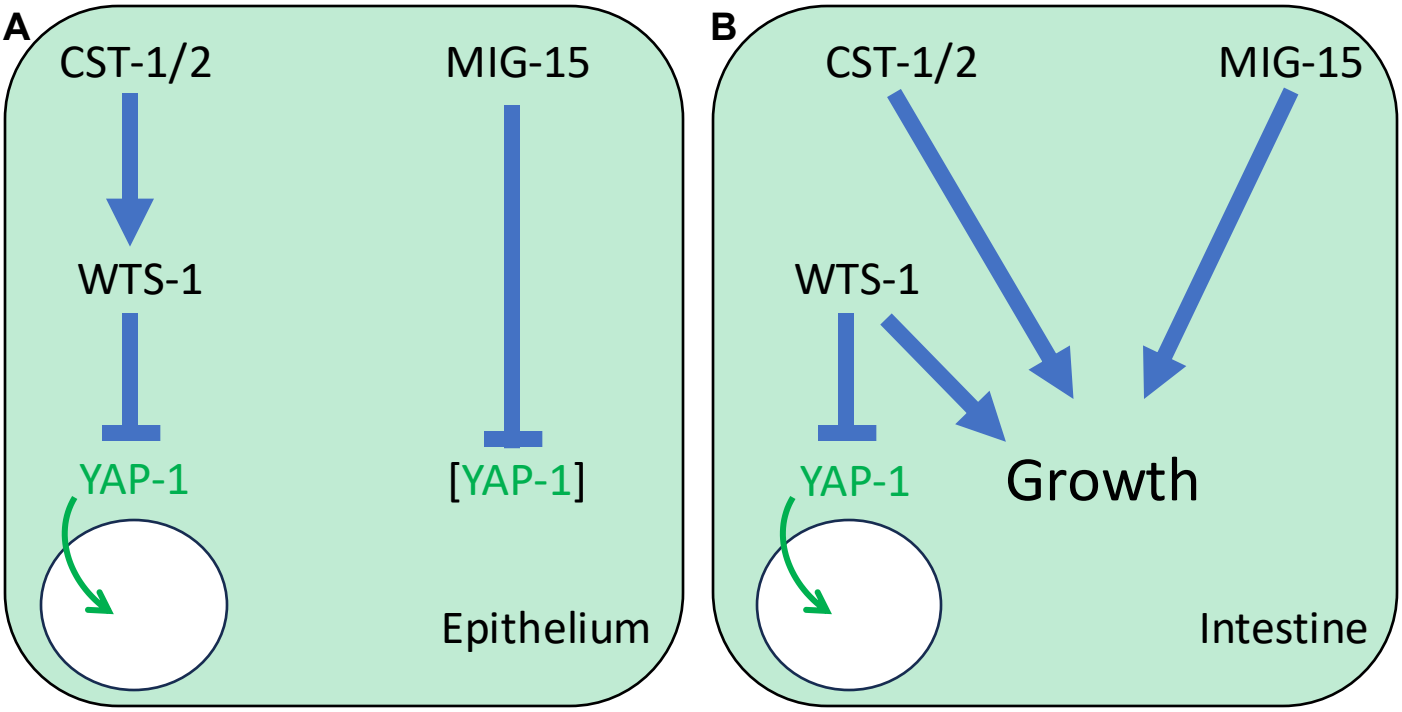
Huynh Figure 7